

## Supporting Information of

### Self-association and Columnar Liquid Crystalline Phase of Cationic Alkyl-substituted-Bipyridine Benzenedithiolato Gold(III) Complexes

Tomohiro Ogawa,<sup>a</sup> Misaki Sakamoto,<sup>a</sup> Hiroataka Honda,<sup>a</sup> Takeshi Matsumoto,<sup>b</sup> Atsushi Kobayashi,<sup>a</sup> Masako Kato<sup>a</sup> and Ho-Chol Chang<sup>c\*</sup>

<sup>a</sup> Department of Chemistry, Faculty of Science, Hokkaido University, North-10, West-8, Kita-ku, Sapporo 060-0810, Japan

<sup>b</sup> Center for Strategic Utilization of Elements, Faculty of Science, Hokkaido University, North-10, West-8, Kita-ku, Sapporo 060-0810, Japan

<sup>c</sup> Department of Applied Chemistry, Faculty of Science and Engineering, Chuo University, 1-13-27 Kasuga, Bunkyo-ku, Tokyo, 112-8551, Japan

#### Contents

- Figure S1.** Concentration dependent <sup>1</sup>H NMR spectra of **3** in chloroform-*d*.
- Figure S2.** Thermogravimetry-differential thermal analyses of **3** and **4**.
- Figure S3.** Differential scanning calorimetry curves of **3**.
- Figure S4.** Variable temperature X-ray diffraction patterns of **3** at 40 °C and 120 °C.
- Figure S5.** Polarized optical microscopy images of **3**.
- Figure S6.** Variable temperature X-ray diffraction patterns of **4** at 25 °C and –80 °C.
- Figure S7.** Cyclic voltammograms of C13bpy and C8,10bpy.
- Figure S8.** Scan rate dependency of cyclic voltammograms of **1** and **2**.
- Figure S9.** Scan rate dependency of cyclic voltammograms of **3** and **4**.
- Figure S10.** Infrared spectra of **1-4**.

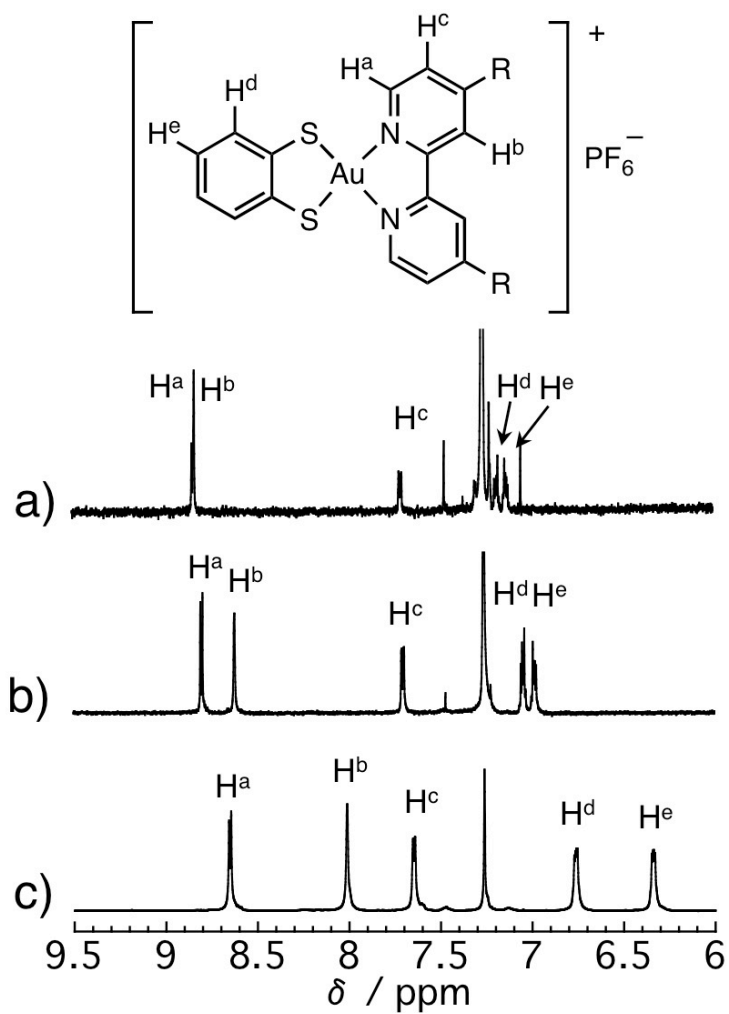


**Figure S1.** Concentration dependent <sup>1</sup>H NMR spectra of **3** in chloroform-*d* at a)  $1.16 \times 10^{-4}$ , b)  $0.96 \times 10^{-3}$  and c)  $0.99 \times 10^{-2}$  M.

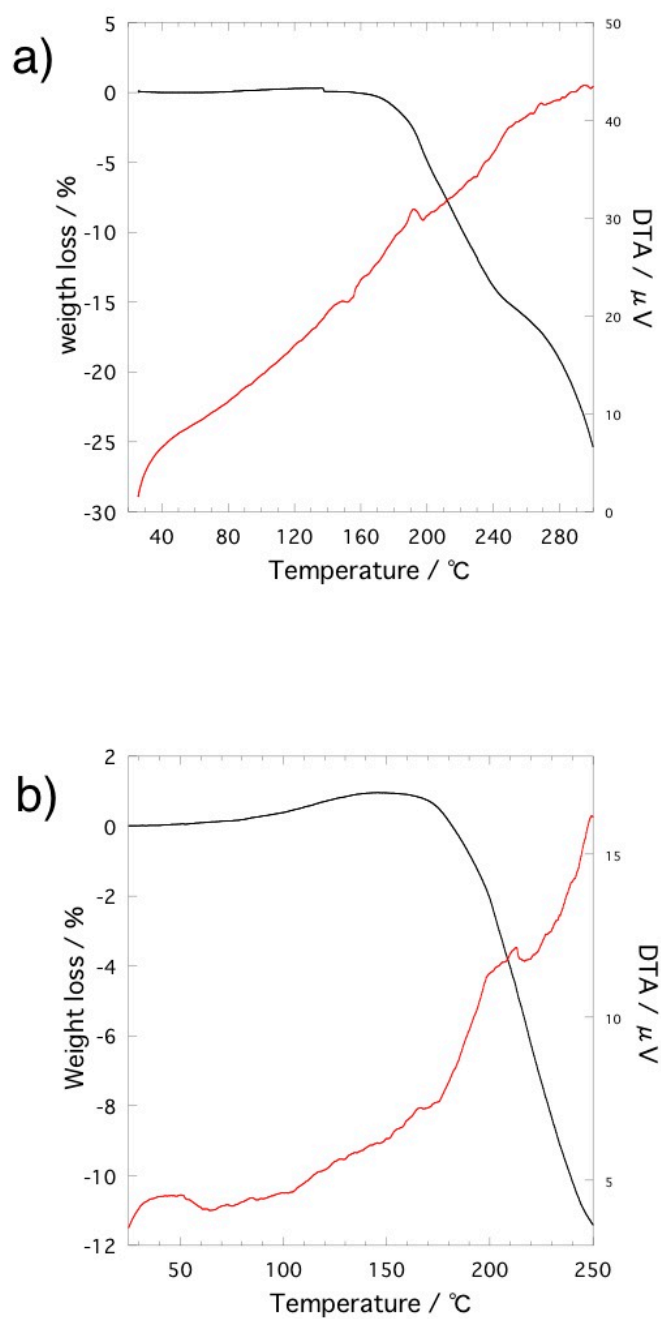


**Figure S2.** Thermogravimetry-differential thermal analyses of a) **3** and b) **4** at scan rate of 5 K/min (TG (–) and DTA (–)).

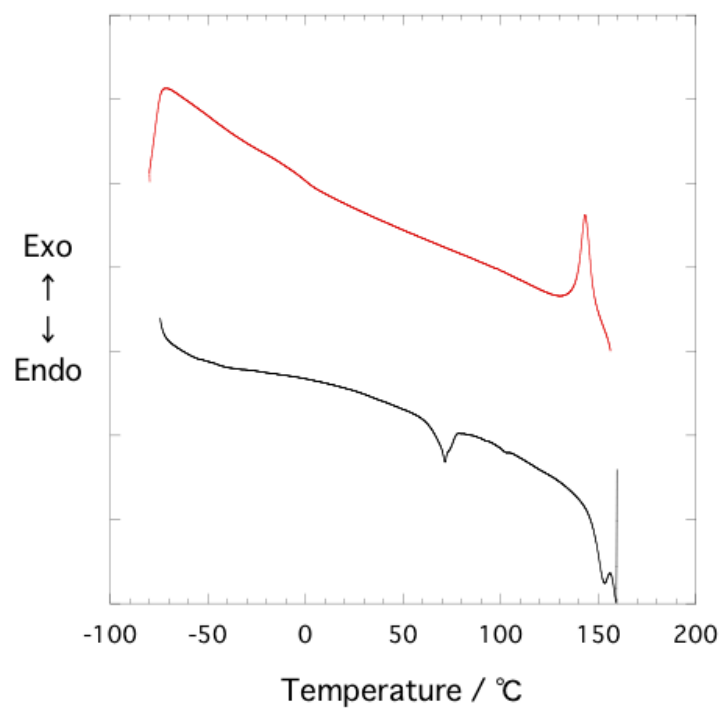


**Figure S3.** DSC curves of **3** at a scan rate of 5 K/min (first heating scan (–) and second cooling scan (–)).

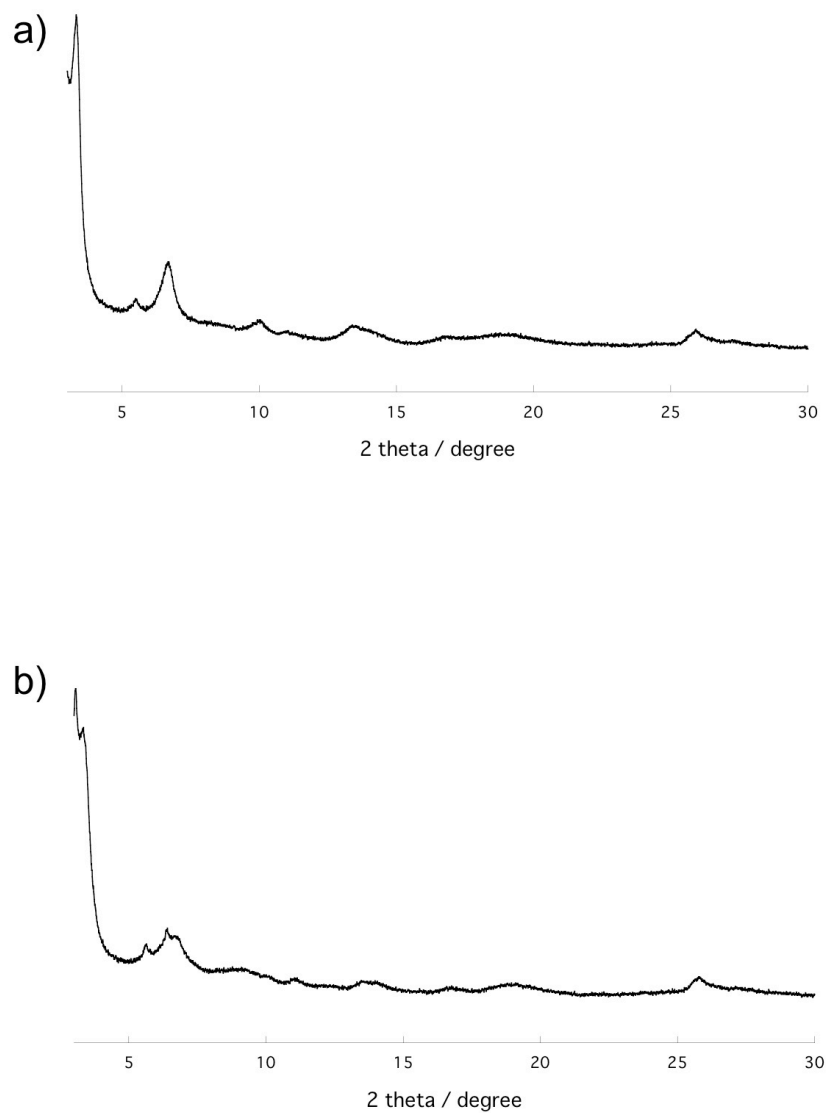


**Figure S4.** Variable temperature X-ray diffraction patterns of **3** at a) 40 and b) 120 °C. Each reflection becomes broad because the complex easily loses its crystallinity. However, the XRD patterns at two temperatures clearly differ from each other, indicating a crystal-to-crystal phase transition.

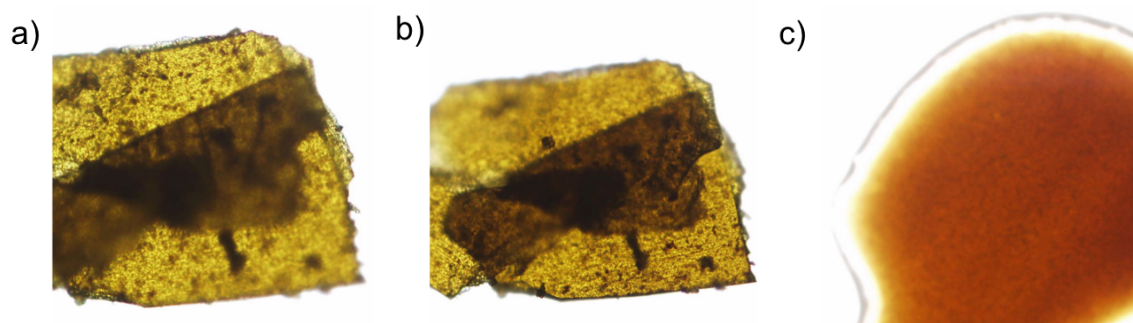


**Figure S5.** POM images of **3** at a) 25 (Cr1), b) 120 (Cr2) and c) 160 °C (Iso).

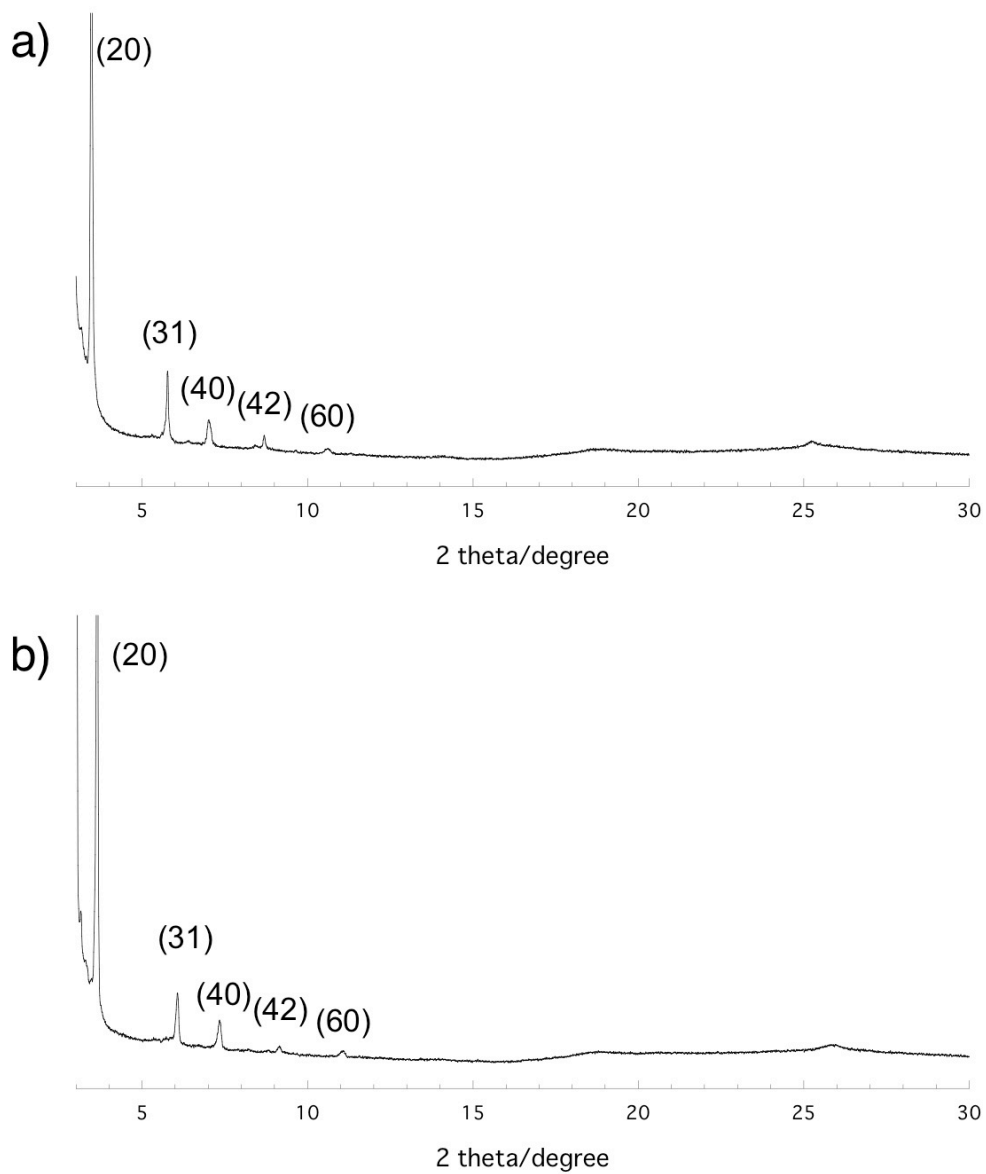


**Figure S6.** Variable temperature X-ray diffraction patterns of **4** at a) 25 and b) -80 °C. The sample was held at 60 °C for four days during the first cooling scan at a scan rate of 5 K/min.

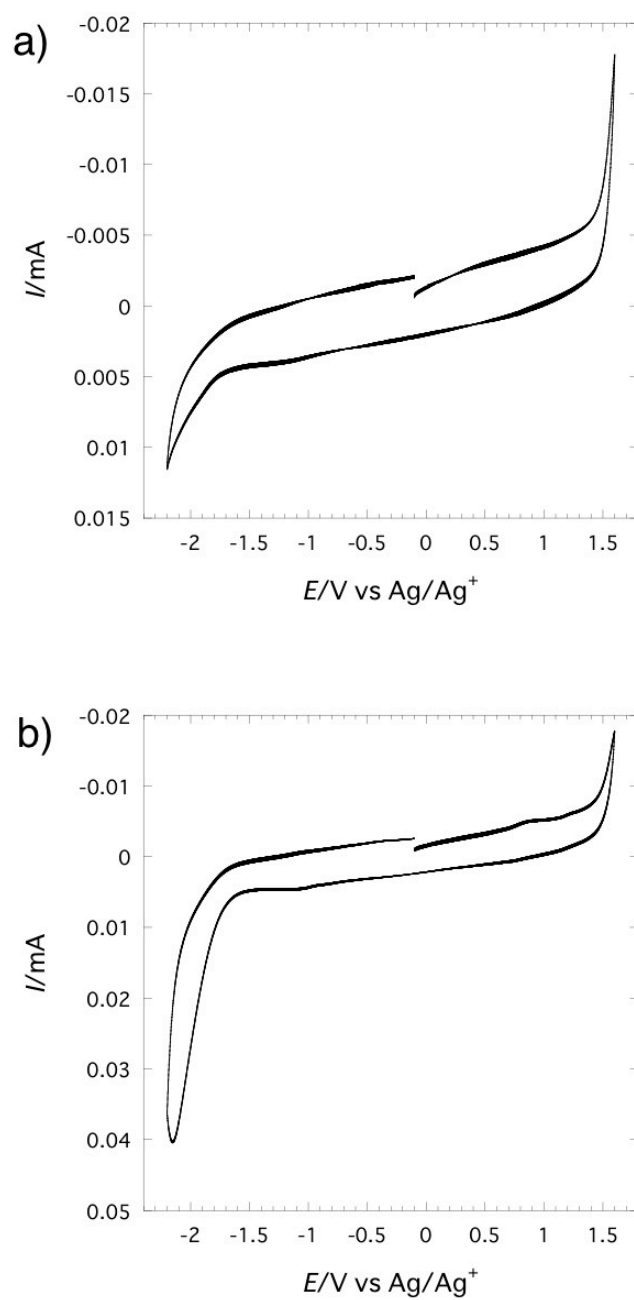


**Figure S7.** Cyclic voltammograms of a) C13bpy and b) C8,10bpy in CH<sub>2</sub>Cl<sub>2</sub> (0.1 M *n*-Bu<sub>4</sub>NPF<sub>6</sub>, N<sub>2</sub>, 100 mV/s).

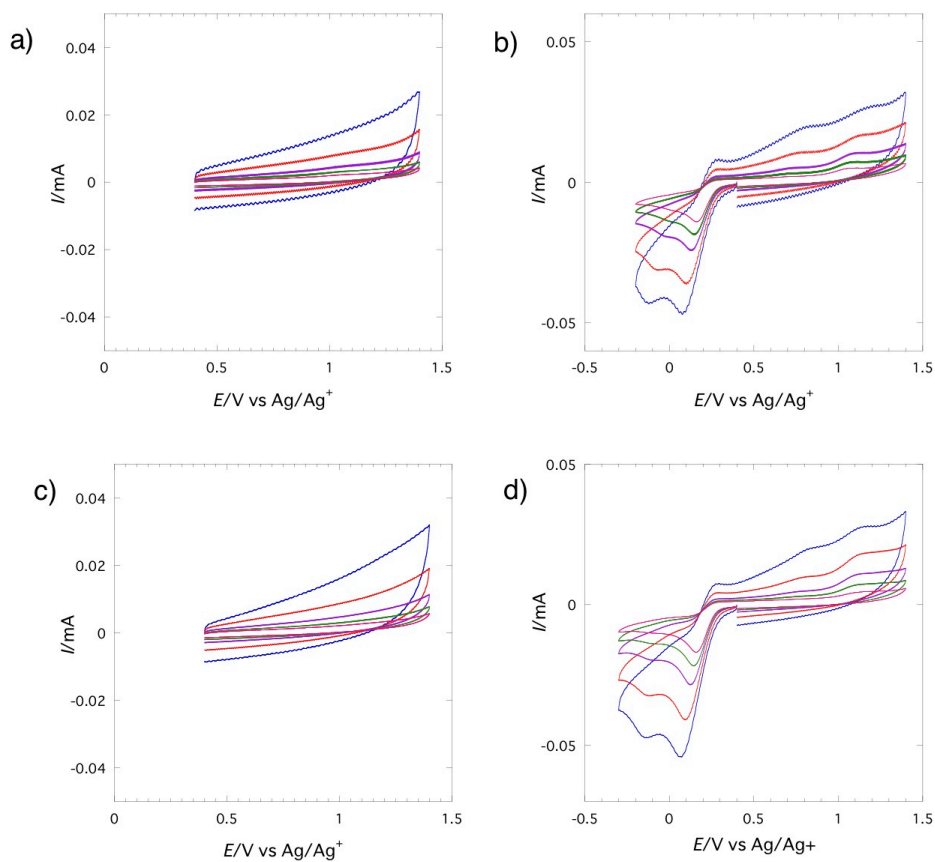


**Figure S8.** Scan rate dependency of cyclic voltammograms of **1** in a) positive scan and b) negative scan and **2** in c) positive scan and d) negative scan in  $\text{CH}_2\text{Cl}_2$  (1000 (–), 500 (–), 200 (–), 100 (–) and 50 mV/s (–), 0.1 M  $n\text{-Bu}_4\text{NPF}_6$ ,  $\text{N}_2$ ).

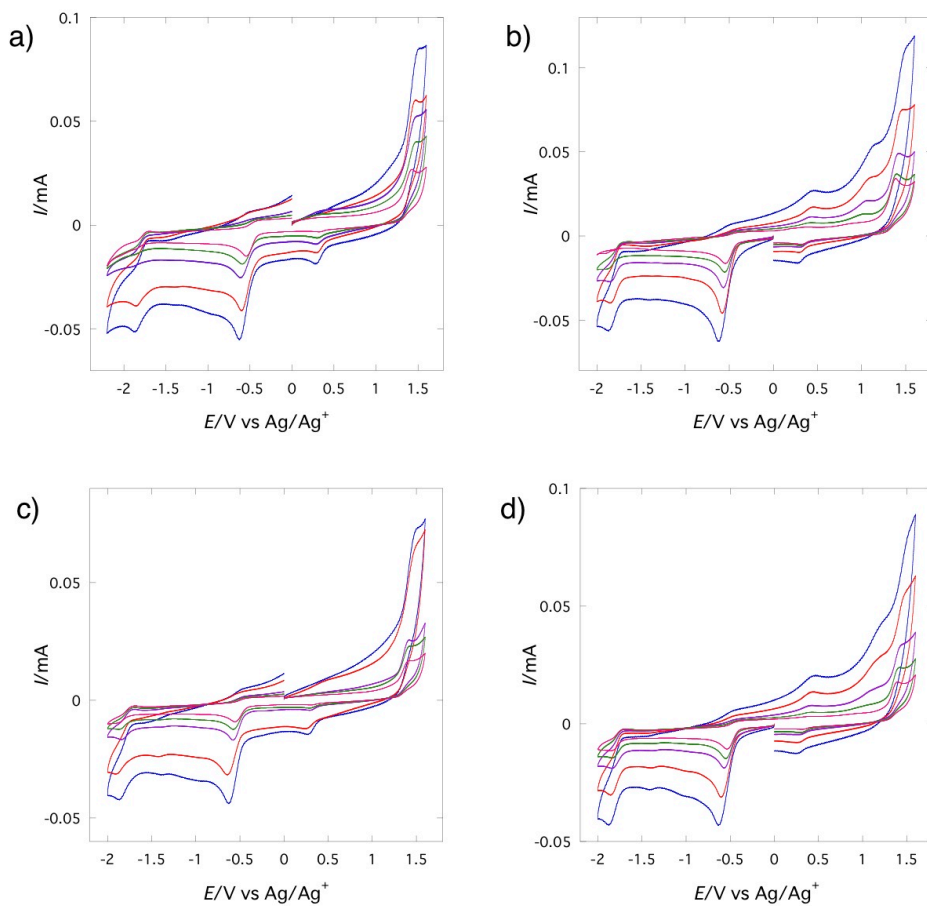


**Figure S9.** Scan rate dependency of cyclic voltammograms of **3** in a) positive scan and b) negative scan and **4** in c) positive scan and d) negative scan in CH<sub>2</sub>Cl<sub>2</sub> (1000 (–), 500 (–), 200 (–), 100 (–) and 50 mV/s (–), 0.1 M *n*-Bu<sub>4</sub>NPF<sub>6</sub>, N<sub>2</sub>).

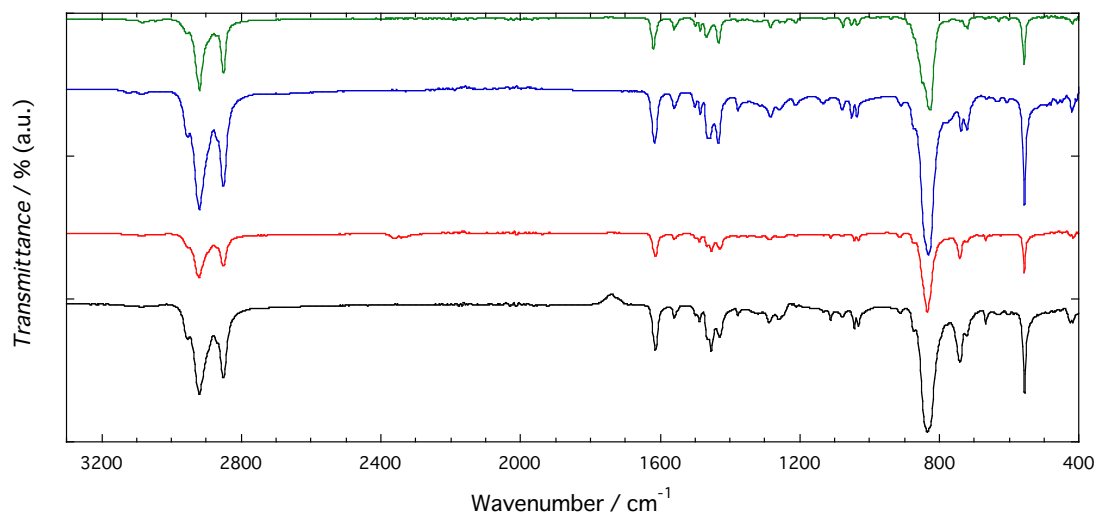


**Figure S10.** Infrared spectra of **1** (–), **2** (–), **3** (–) and **4** (–).